Gallium Sulfide Quantum Dots with Zinc Sulfide and Alumina Shells Showing Efficient Deep Blue Emission

Avijit Saha, Ranjana Yadav, Dmitry Aldakov, Peter Reiss

RESEARCH ARTICLE

Gallium Sulfide Quantum Dots with Zinc Sulfide and Alumina Shells Showing Efficient Deep Blue Emission

Avijit Saha,[a] Ranjana Yadav,[a] Dmitry Aldakov,[a] Peter Reiss[a,*]

In memory of Dr. Andreas Eichhöfer.

[a] Dr. Avijit Saha, Dr. Ranjana Yadav, Dr. Dmitry Aldakov, Dr. Peter Reiss
IRIG-SyMMES
Univ. Grenoble Alpes, CEA, CNRS
38000 Grenoble, France
E-mail: peter.reiss@cea.fr

Supporting information for this article is given via a link at the end of the document.

Abstract: Solution-processed quantum dot (QD) based blue emitters are of paramount importance in the field of optoelectronics. Despite large research efforts, examples of efficient deep blue/near UV-emitting QDs remain rare due to lack of luminescent wide bandgap materials and high defect densities in the existing ones. Here, we introduce a novel type of QDs based on heavy metal free gallium sulfide (Ga_2S_3) and their core/shell heterostructures Ga_2S_3/ZnS as well as Ga_2S_3-ZnS-Al_2O_3. The PL properties of core Ga_2S_3 QDs exhibit various decay pathways due to intrinsic defects, resulting in a broad overall PL spectrum. We show that the overgrowth of the Ga_2S_3 core QDs with a ZnS shell results in the suppression of the intrinsic defect mediated states leading to efficient deep-blue emission at 400 nm. Passivation of the core/shell structure with amorphous alumina yields a further enhancement of the photoluminescence quantum yield approaching 50% and leads to an excellent optical and colloidal stability. Finally, we develop a strategy for the aqueous phase transfer of the obtained QDs retaining 80% of the initial fluorescence intensity.

Introduction

Research on colloidal semiconductor QDs has been tremendously expanded in the last decades fuelled by their outstanding photophysical properties and solution processability, making them suitable for many domains of applications, such as photocatalysis,[1] optoelectronics,[2] biological applications,[3] and more recently, quantum technologies.[4] In particular, Pb- and Cd-based materials have been widely studied due to their high photoluminescence quantum yield (PLQY), tunability and color purity and have been integrated into numerous optoelectronic devices.[5] However, the presence of toxic heavy metals (Pb, Cd) severely limits the translation from research to real-life applications. Recent years have therefore seen a growing interest in heavy metal-free semiconductor QDs,[6] such as III-V-based InP QDs,[2c, 7] I-III-VI_2-based chalcopyrites such as $CuInS_2$, $CuInSe_2$, $AgInS_2$,[8] and halide perovskite nanocrystals,[9] all of which show a high potential as visible light emission. However, despite this variety of materials, very few examples exist [10] covering the deep blue and near UV (400 nm or below) part of the spectrum. Such wide bandgap, efficient UV emitters are of paramount importance in various fields of applications, such as UV-LEDs, photocatalysis and biotechnology.[11]

Recently, the III-VI material Ga_2S_3 emerged as a potential blue emitter because of its wide direct bandgap ranging from 2.5 to 3.4 eV depending on the crystal structure and defects.[12] Gallium sulfide is also an emerging shell material for QDs, in particular for $AgInS_2$, giving rise to unprecedented optical properties of the latter.[8b, 8c, 13] The optical properties of Ga_2S_3 single crystals have been explored at low temperatures[14] revealing that the luminescence arises from the recombination of donor and acceptor levels caused by S and Ga vacancies, respectively.[15] Ga_2S_3 exhibits polymorphism: only the monoclinic α-phase is stoichiometric, while the hexagonal β- and cubic γ-phases are sulfur-deficient.[16] Thus, the control of the crystal structure and stoichiometry are important parameters directly influencing the emission properties of Ga_2S_3 in the bulk and at the nanoscale. To date, there is only one report related to Ga_2S_3 QDs, which shows tunable broad emission depending on the stoichiometric Ga/S feed ratio.[17] The broad emission consists of several peaks which were attributed to different optical transitions. Ga_2S_3 is a natural defect semiconductor and these different transitions are occurring from radiative donor-acceptor pair (DAP) like recombination processes, which originate from the intrinsic defects.[14, 18] Understanding the defect-mediated donor-acceptor levels and recombination dynamics occurring through these channels has pivotal importance to achieve narrow-width single-component emission.

Herein, we introduce a synthetic method providing precise control over these defects to monitor the specific optical transition. Moreover, we passivate the defect states using a ZnS shell to suppress all other optical transitions and selectively enhance the band-edge emission near 400 nm. This allows us to achieve intense comparatively narrow-band deep-blue emission, which was not observed before in gallium sulfide-based materials. In

addition, we have developed a versatile approach to improve the environmental stability of these QDs by growing an amorphous alumina (Al_2O_3) shell on top. Alumina is chemically inert and prevents the degradation of the QDs in different environments as well as the associated leaching out of metal ions, which can have toxic effects (e.g., zinc).[19] Moreover, a thin layer of alumina has been shown to be beneficial in optoelectronic applications (e.g., photodetectors) to passivate the active layer or in photocatalysis to protect the active material and reduce undesired recombination processes.[20] Here, we report for the first time synthesis of $Ga_2S_3/ZnS/Al_2O_3$ core/shell/shell QDs and discuss their recombination dynamics via various decay channels using control experiments. Finally, we establish a generic solution-phase ligand exchange protocol to transfer the alumina-coated QDs into water while maintaining their strong luminescence.

Results and Discussion

Ga_2S_3 QDs were synthesized as described in the experimental section using a one-pot heat-up approach. The optical properties of the QDs could be tuned with the reaction time (cf. Figure 1a). After 5 min, we observe a small shoulder peak in the UV-vis absorption spectra before the absorption edge, which could be due to the size distribution at the initial growth stages of the Ga_2S_3 QDs.

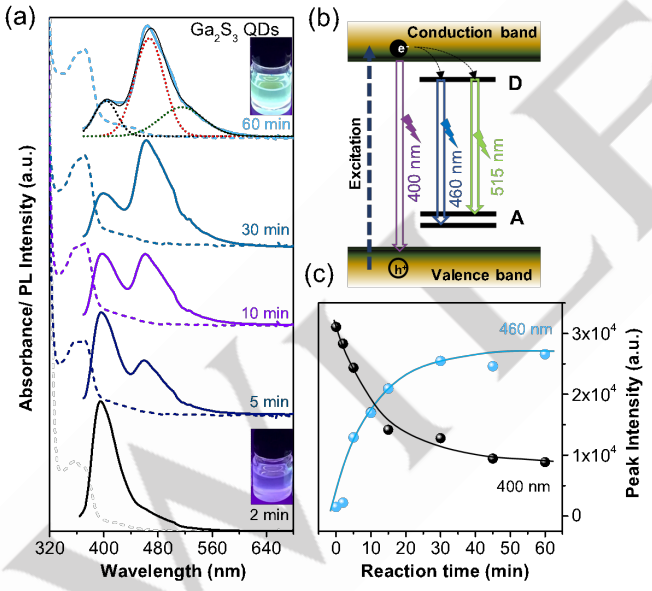

Figure 1. (a) Absorption (dashed lines) and PL (solid lines) spectra of Ga_2S_3 QDs dispersed in toluene obtained for different reaction times at 280 ºC. All PL spectra were measured with an excitation wavelength of 350 nm. The insets show the 2 min and 60 min samples exhibiting blue and greenish emission, respectively, under UV light. Ga_2S_3 60 min PL peak has been deconvoluted with three Gaussian peaks (short dots) and a thin black line shows the cumulative fit (b) Schematic representation of the energy levels of the Ga_2S_3 QDs and the possible recombination pathways due to band edge and vacancy related donor and acceptor states. (c) Temporal evolution of the PL peak intensities of the peak near 400 nm (black) and that at 460 nm (blue).

For longer reaction times (30/60 min), a single, pronounced absorption peak at around 380 nm is evolving. Concerning the emission properties, it is evident from Figure 1a that there is an evolution of three different types of transitions resulting in three PL signals near 400, 460, and 515 nm (shoulder), respectively, depending on the reaction time. Based on reported results on bulk crystals of Ga_2S_3,[14] Figure 1b proposes a hypothetical scheme of the involved recombination channels of the photogenerated carriers, which show different transition probabilities. III-VI compounds (Ga_2S_3, In_2S_3) are known as natural defect semiconductor because of their high density of crystal defects originating from their synthesis.[18, 21] The defect states are caused by sulfur and gallium vacancies which behave as donor (D) and acceptor (A) sites, respectively.[18] In the S-deficient composition of the QDs, sulfur vacancies are naturally present, while gallium vacancies are formed due to the requirement of charge equilibrium. It is apparent from Figures 1a and 1b that the PL peak near 400 nm is due to band edge emission while the peaks at 460 and 515 nm are the results of defect-related mid-gap emissions due to donor-acceptor pair recombination. Unlike previous reports, we do not observe any broad emission bands. Instead, we are able to observe comparatively distinct emission peaks resulting from the different recombination pathways. At the initial stage of the sample growth (1-2 min at 280 ºC), the sharp band-edge peak at 395 nm dominates over the other peaks suggesting the insignificant presence of the vacancy-related mid-gap states. However, with increasing reaction time, the peak at 460 nm along with a shoulder peak at 515 nm slowly evolve under concomitant decrease of the band-edge peak as depicted in Figure 1c. It is noteworthy that both the absorption peak and the highest energy PL peak (near 400 nm) show a consistent redshift with reaction time: the absorption one from 370 to 376 nm, and the PL one from 395 to 402 nm. On the contrary, the PL peaks at 460 and 515 nm remain unaltered in their respective positions. These results support the assignment of the highest energy peaks to band-edge absorption/emission, showing a small redshift with the reaction time due to QD growth as a result of weak quantum confinement effects, whilst the peaks at 460 and 515 nm are due to the mid-gap states, which are not sensitive to size variation.

To get more insights into the origin of the sub-bandgap and bandgap transitions and the radiative processes, we performed photoluminescence excitation (PLE) spectroscopy. Figure S1a (Supporting information (SI)) shows the PLE scans of the Ga_2S_3 QDs annealed for 30 min at 280°C, measured for the PL peaks at 410 and 470 nm, respectively. The PL excitation spectra look very similar to their corresponding absorption spectra, suggesting that while emission mostly occurs through the mid-gap states, light absorption is dominated by the host semiconductor's bandgap. However, another peak at around 440 nm is observed in the PLE spectra due to sub-bandgap excitation involving Ga and S defects as observed earlier.[22] To understand the exciton decay dynamics and the recombination pathways inside the QDs, we performed time-resolved PL (TRPL) analyses (Figure S1c). For these measurements, the samples were excited with a pulsed NanoLED emitting at 350 nm and the decay was monitored at the 400 and 460 nm emission wavelengths. While the mid-gap emission at 460 nm has multiple decay pathways resulting in a bi-exponential

decay behavior, the band-edge emission monitored at 400 nm has single-exponential nature. The PLQY of the as-synthesized Ga_2S_3 QDs is remarkably high (10-15%), and the PL emission can easily be seen under a UV lamp (cf. Inset of Figure 1a). To further increase the PL efficiency, we explored the passivation of the QDs' surface with a wider bandgap semiconductor by growing a ZnS shell. As mentioned above, it is possible to have two distinct emission wavelengths (at around 400 and 460 nm) from the Ga_2S_3 core QDs depending on the reaction time. Therefore, in two separate experiments, we have grown ZnS shells on the two different Ga_2S_3 core QDs, showing either band-edge or mid-gap emission. Moreover, to enhance the chemical stability, a thin shell of amorphous alumina has been grown on top of the ZnS shell.

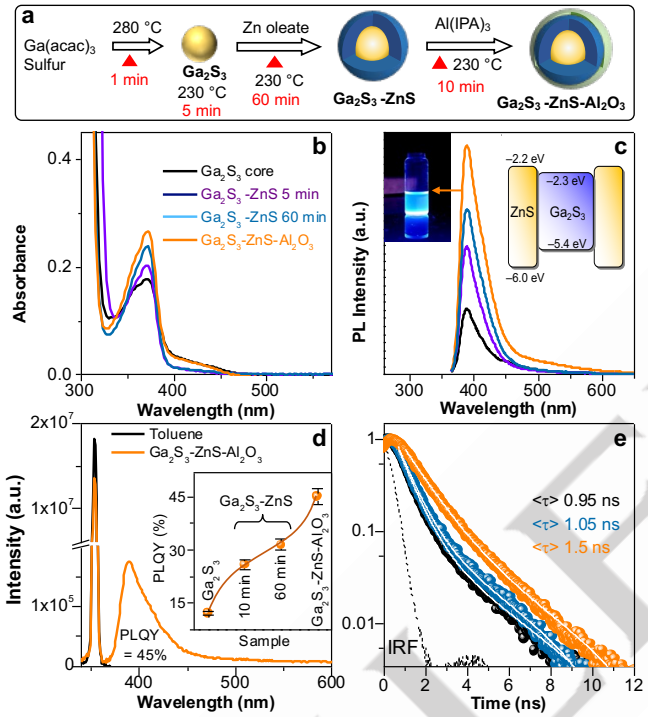

Figure 2. (a) Schematic of the synthesis method used for preparing Ga_2S_3 core, Ga_2S_3/ZnS core/shell, and Ga_2S_3/ZnS/Al_2O_3 core/shell/shell QDs. (b) Absorption and (c) PL (normalized for absorbance at the excitation wavelength of 350 nm) of the core Ga_2S_3 (black), Ga_2S_3/ZnS core/shell (violet and blue) and Ga_2S_3/ZnS/Al_2O_3 core/shell/shell QDs (orange). The insets show the photograph of the Ga_2S_3-ZnS-Al_2O_3 QDs under UV radiation and the band alignment of the Ga_2S_3/ZnS QDs forming a type-I heterostructure. (d) Absolute PLQY measurement of Ga_2S_3-ZnS-Al_2O_3 QDs. The sharp peaks at 355 nm show the scattering of Toluene (black) and QDs (orange) dispersed in toluene while the peak at 400 nm shows the effective sample emission after removing the background emission from toluene. The inset depicts the variation of the PLQY at the different synthesis stages. (e) PL decay curves (excited at 350 nm) of the core, core/shell and core/shell/shell QDs. The decay spectra were fitted with bi-exponential functions and the calculated average lifetimes are displayed (IRF: instrument response function).

While the details of the shell overcoating have been described in the experimental section, Figure 2a schematically shows the overall synthesis method for Ga_2S_3 core QDs with dominating band-edge emission. Figure 2b and 2c show the evolution of the UV-VIS absorption and PL spectra, respectively, from the core over various stages of ZnS growth and after alumina overcoating. During the ZnS growth, the absorption and PL peak does not show any redshift indicating the formation of a type-I semiconductor heterostructure. Photoelectron yield spectroscopy in air (PYSA) resulted in a valence band maximum of –5.4 eV. Using the optical band gap of the Ga_2S_3 QDs and the reported band positions of ZnS allows constructing the energy level scheme depicted in Fig. 2c (inset). No secondary absorption peak of ZnS QDs can be detected, suggesting the formation of a ZnS shell rather than separate nucleation. The spectral shape with a single sharp peak at around 380 nm exhibiting a higher energy shoulder is also preserved after overgrowth with the alumina shell, while in this case also a small absorption in the 400-425 nm range reappears, similar to the Ga_2S_3 core QDs. All QDs exhibit deep blue emission near 400 nm. The PLQY significantly improved with the growth of the ZnS and was further enhanced with alumina overcoating. PLQY measurements using an integrating sphere were performed to obtain the absolute values as illustrated in Figure 2d, while the variation of the PLQY for the different structures (core, core/shell, core/shell/shell) is monitored in the inset of Figure 2d. The PLQY of the core Ga_2S_3 QDs (12.2 ± 0.6%), improved with the growth of the ZnS layer up to 31.4 ± 1.6 %, and was further enhanced up to 45± 2.3 % in the case of the Ga_2S_3/ZnS/Al_2O_3 QDs. This strong enhancement in the PL intensity is attributed to the removal of defects by surface passivation with the ZnS shell and finally with the Al_2O_3 matrix. To investigate the effect of surface passivation induced by the ZnS shell, we performed a control experiment on Ga_2S_3 core QDs having dominant defect related mid-gap emission at 460 nm. We note that the ZnS growth leads to the selective suppression of the 460-nm and 515-nm emission peaks and to the concomitant strong enhancement of the 400-nm peak (Figure S2a, SI). The origin of these changes is visualized in the schematic shown in Figure S2b (SI). The growth of the ZnS shell leads to the suppression of surface states which are responsible for the radiative mid-gap state emission and other non-radiative decays in Ga_2S_3 QDs resulting in the enhanced recombination through band-edge states and an overall increase of the PLQY as depicted in Figure S2c (SI). This behavior indicates that the mid-gap states originated from the Ga and S vacancies form predominantly on the surface rather than in the bulk of the Ga_2S_3 QDs. In addition to the enhanced PLQY, these QDs show a PL linewidth (full width at half maximum) of the band-edge peak (38 nm), which remains invariant to the ZnS and alumina shell growth (Figure 2c). The PL lifetimes (Figure 2e) fitted with bi-exponential functions remained similar for all samples. Nonetheless, an increase in the average lifetime is observed when going from the core (0.95 ns), to the core/shell (1.05 ns) and core/shell/shell (1.51 ns) QDs indicating the decreased contribution of fast non-radiative decay channels, which also manifests by the more single-exponential behavior observed with the alumina shell (cf. Table S1, SI).

Long-term colloidal and optical stability is an essential factor for the application of QDs, which is commonly limited by the alteration or degradation of the QDs' surface. The bare Ga_2S_3 QDs have

poor colloidal stability (a few days), while the Ga_2S_3/ZnS core-shell and Ga_2S_3-ZnS-Al_2O_3 core-shell-shell QDs remain stable for months. To investigate the stability of the optical properties, we studied the evolution of the PL of the three different types of QDs for a month while storing them under ambient conditions, namely as colloidal solutions of identical concentrations in toluene (non-anhydrous) and without any precautions to avoid their exposure to air. As expected (Figure 3), all QDs lose part of their emission efficiency with time, however, the Ga_2S_3/ZnS QDs exhibit a significant enhancement of the optical stability compared with the Ga_2S_3 core QDs, which was further improved after Al_2O_3 overcoating. Figure 3d demonstrates that after one month, Ga_2S_3 QDs lose 60% of the initial PL efficiency, Ga_2S_3/ZnS about 20% and Ga_2S_3/ZnS/Al_2O_3 core/shell/shell QDs only about 10%. Hence, the combined surface passivation using ZnS and alumina results in the best preservation of the optical properties and provides a highly appealing strategy for increasing the shelf life of this type of QDs.

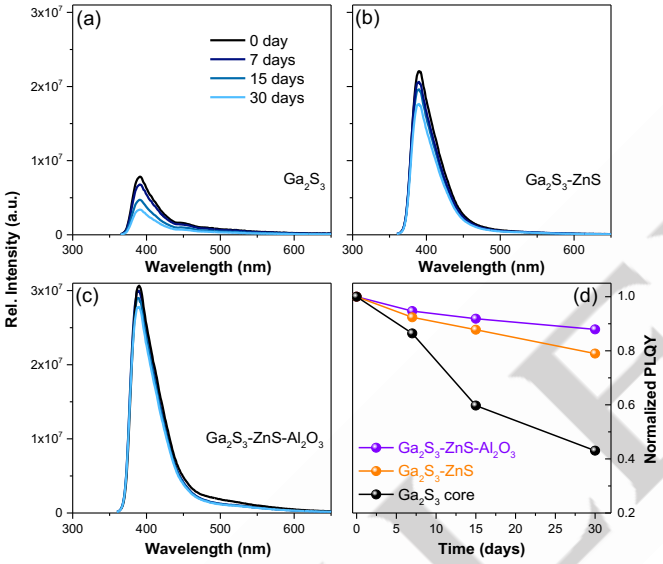

Figure 3. Evolution of the PL spectra with time after synthesis (after 0, 7, 15, and 30 days) of (a) Ga_2S_3 core, (b) Ga_2S_3/ZnS core/shell, and (c) Ga_2S_3/ZnS/Al_2O_3 core/shell/shell QDs. (d) Temporal evolution of PLQY relative to the starting value just after synthesis.

Figure 4 shows low-magnification, bright-field transmission electron microscopy (TEM) images of the Ga_2S_3 core QDs before and after the growth of the ZnS and Al_2O_3 shells. All three types of QDs are exclusively constituted of light elements, which makes their TEM analysis intrinsically difficult. Nonetheless, the image analysis using different areas revealed that the core QDs have a quasi-spherical morphology and a low size distribution with a diameter of 2.8±0.7 nm (Figure 4a), which increased to 3.85±0.6 nm (Figure 4b) and 4.3±0.6 nm (Figure 4c) after ZnS and alumina shell growth, respectively. The unaltered morphology, uniform diameter increases of the QDs and absence of any other separate size distribution suggests the homogeneous shell growth on the Ga_2S_3 core QDs. Structural analyses have been performed using powder X-Ray diffraction (XRD) as shown in Figure S3 (SI). Due to the small crystallite size and eventually amorphous nature, the diffraction peaks of the Ga_2S_3 core QDs are very broad and of low intensity, impeding further analysis. The intense peak at around 20° (2 theta) is attributed to the contribution of excess organics (cf. below). After the growth of the ZnS shell, the diffractogram is dominated by the aforementioned 20° peak as well as broad features around 35 and 60°. These cannot be assigned to known phases of Ga_2S_3 or $ZnGa_xS_y$ and hence indicate the formation of a new gallium sulfide phase. The remaining lower-intensity signals at 28 and 47° coincide with the positions of the (111) and (220) peaks of cubic ZnS (cf. Fig. S3). However, this is only a tentative assignment, as the ZnS shell thickness is just 0.5 nm, i.e., the size of one unit cell. The large lattice mismatch between Ga_2S_3 and ZnS impedes epitaxial shell growth, likely yielding an imperfect ZnS shell. The Al_2O_3 overcoating did not lead to distinct changes in the diffraction pattern, suggesting the formation of a thin, amorphous layer on top of the core-shell QDs without the generation of secondary phases or separate alumina particles.

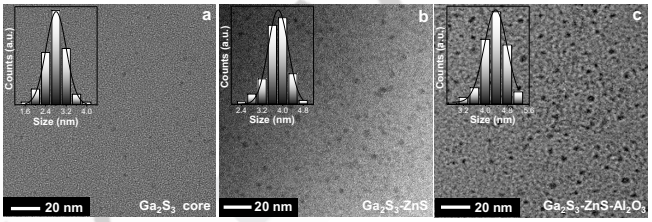

Figure 4. Bright-field TEM images of (a) Ga_2S_3 core, (b) Ga_2S_3/ZnS core/shell, and (c) Ga_2S_3/ZnS/Al_2O_3 core/shell/shell QDs. The insets show the size distribution histograms.

XPS analysis has been performed to investigate the chemical states of the constituting elements and the composition of the QDs. Figures 5a and 5b represent the high-resolution XPS spectra of Ga $2p_{3/2}$ and S 2p. The ratio between the integrated intensity of Ga 2p and S 2p is 2:3.5, which suggests the formation of Ga_2S_3 QDs with a slightly sulfur-rich surface. For further information, the spectra have been deconvoluted considering the spin-orbit splitting where the binding energy differences, full width at half maximum (FWHM), and area under the curve are fixed using standard values from the database. The Ga $2p_{3/2}$ signal can be deconvoluted into two peaks assigned to the Ga-S and Ga-O bond. The small contribution of Ga-O is due to the oxidation of Ga at the QD surface likely occurring during sample purification and transfer. In the S2p spectrum (Figure 5b), the deconvoluted doublet peaks are located at 160.73 and 161.89 eV with a peak separation of 1.16 eV, consistent with the expected values in the sulfide phase and confirming the formation of gallium sulfide QDs. Figures 5c, 5d and 5e show the high-resolution XPS spectra for Ga$2p_{3/2}$, S2p and Zn $2p_{3/2}$ of the Ga_2S_3/ZnS core/shell QDs. Unlike the Ga $2p_{3/2}$ spectrum of the Ga_2S_3 core QDs (Figure 5a), the core/shell QDs (Figure 5c) do not display the peak related to Ga-O. Therefore, it can be concluded that the in-situ formation of the ZnS shell effectively prevents the surface oxidation of the Ga_2S_3 core QDs. The similar, single S $2p_{3/2}$ and S $2p_{1/2}$ doublet signal (Figure 5d) confirms, as expected, the presence of S in the sulfide phase for both core and shell parts. Finally, the presence of the Zn $2p_{3/2}$ peak (Figure 5e) further confirms the formation of ZnS. Thus, the presence of ZnS revealed by XPS, along with the

uniform size growth from TEM images, confirms the successful formation of the ZnS shell on the surface of the Ga_2S_3 core QDs, which gives rise to superior optical properties as shown above.

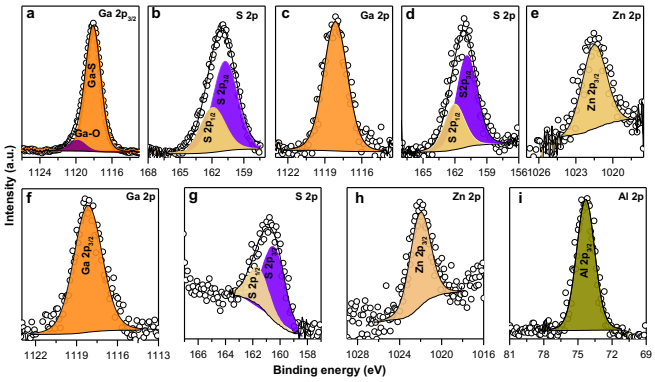

Figure 5. High resolution XPS spectra of (a-b) Ga_2S_3 core (c-e) Ga_2S_3/ZnS core/shell and (f-i) Ga_2S_3/ZnS/Al_2O_3 core/shell/shell QDs.

To confirm the presence of the alumina shell, XPS measurements and analysis were also performed for the Ga_2S_3/ZnS/Al_2O_3 QDs. Figure 5(f-i) shows the high resolution XPS spectra for Ga $2p_{3/2}$, S 2p, Zn $2p_{3/2}$ and Al 2p, respectively. While the Ga, S, and Zn peaks are very similar to those in the Ga_2S_3/ZnS QDs, in additional strong Al 2p peak can be detected. The Al 2p core level presents the clear signature of Al^{3+} and confirms the presence of the Al_2O_3 shell. A composition analysis from the XPS studies of all three samples is summarized in Table S2 (SI).

The ligand environment around the QDs was studied using NMR and FTIR spectroscopy. Figure S4 (SI) presents the proton NMR spectra of the QDs dispersed in $CDCl_3$. We observe the presence of ODE (chemical shifts indicated in the figure) in all the samples as ODE has been used as an organic solvent for the synthesis. Due to the high temperatures used, ODE polymers may form, which cannot be easily removed from the surface during the QD purification.[23] NMR also reveals that TBP is attached to the surface, in particular in the case of the core QDs. It is well known that the L-type ligand TBP prefers to bind with the anion sites and therefore leads to the sulfur-rich surface in core Ga_2S_3 QDs as observed from XPS elemental analysis. Furthermore, the presence of oleate ligands (signal of the C=C double bond at 5.27 ppm) arising from Zn-oleate added in the second step of the reaction, is detected in the core/shell and core/shell/shell QDs. The FTIR spectra (Figure S5, SI) of all the samples show the characteristic C-H stretching peaks at 2921 and 2853 cm^{-1}, respectively, due to the presence of the long alkyl chains in the capping ligands. The $-COO^-$ vibration is only detected in the core/shell and core/shell/shell QDs which is consistent with the NMR results.

Finally, we developed a procedure for the aqueous phase transfer of the alumina-capped core/shell/shell samples, which opens the way for their use in biomedical applications and studies. It consists of the phase transfer ligand exchange reaction induced by mixing the pristine QDs in the organic phase (chloroform) with an appropriate surface ligand in the aqueous phase (cf. Experimental Section and Figure 6a). Initial tests with established hydrosoluble bifunctional ligands failed (e.g., cysteine, penicillamine, glutathione, 3-mercaptopropionic acid, etc.) as the thiol does not provide a strong interaction with the surface of the alumina-capped QDs. Therefore, we selected 2-aminoethylphosphonic acid, which can strongly bind to oxide surfaces via the phosphonic acid moiety. As shown in the FTIR spectra in Figure 6b, the intensities of the bands stemming from the pristine surface ligands, visible at 2925 and 2854 cm^{-1} (stretching vibrations of $-CH_2-CH_3$ and $-CH_2-CH_2-$) as well as at 1536 and 1432 cm^{-1} (asymmetric and symmetric stretching vibrations of the $-COO^-$ groups), completely disappear after ligand exchange. Only two new bands assigned to the P=O and P−OH stretching vibrations are visible strongly corroborating the efficient replacement of the hydrophobic organic ligands with water-compatible 2-aminoethylphosphonic acid. In addition to the alumina-capped core/shell/shell QDs, the same procedure also enabled the successful aqueous phase transfer of the ZnS-capped core/shell QDs. Comparison of absorption spectra reveals a slight broadening of the spectral features of the QDs in the aqueous phase compared to the organic phase. However, no broadening in the PL peaks was observed and moreover, the presented procedure does not lead to a strong decrease of the PL intensity as it is ubiquitously observed in phase-transfer ligand exchange procedures of QDs, retaining in the aqueous phase 75-80% of the initial PLQY.

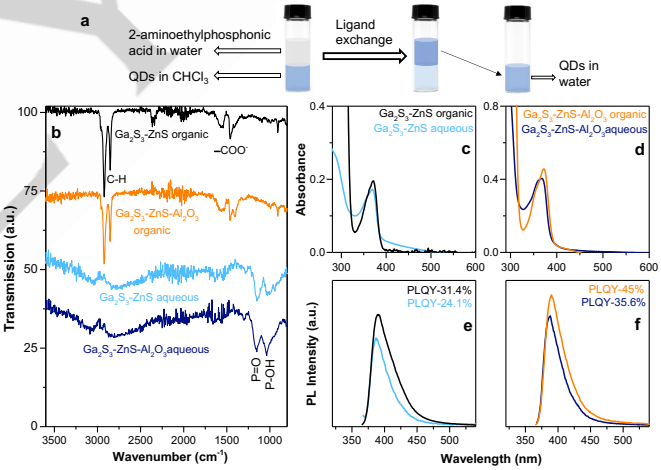

Figure 6. Schematic representation of the aqueous phase transfer of the core/shell and core/shell/shell QDs. (b) FTIR, (c) Absorption, (c) PL spectra of Ga_2S_3/ZnS and Ga_2S_3/ZnS/Al_2O_3 QDs before and after phase transfer ligand exchange.

Conclusion

Summarizing, a synthetic method for producing deep-blue luminescent environmentally friendly Ga_2S_3 QDs has been devised. The study of their photophysical properties revealed that the emission from these QDs can occur through band edge and vacancy (Ga and S vacancy) mediated mid-gap states. The luminescence wavelength can be shifted from 400 to 460 nm by increasing the reaction time, which induces the predominant recombination via mid-gap defect states. The growth of a ZnS

shell on the surface of the Ga_2S_3 QDs passivates the surface and gives rise to a strong enhancement of the band edge emission. The analysis of the optical properties of core/shell QDs obtained from two different types of core QDs demonstrated that the Ga and S vacancies in the core are mostly located on the surface of the QDs rather than in the bulk. Finally, to enhance the chemical and photostability of these core/shell QDs and render them compatible with biological studies, an amorphous alumina shell has been grown. The resulting Ga_2S_3/ZnS/Al_2O_3 core/shell/shell QDs show excellent optical properties, namely a single intense emission with enhanced PLQY compared to Ga_2S_3/ZnS QDs, a well-defined absorption peak and, most importantly, long-term chemical and optical stability in ambient atmosphere. From a fundamental perspective, we have studied the role of vacancies in the mid-gap state emission in the emerging class of III-VI semiconductors and introduced a way to obtain defect-free band-edge emission by developing a novel core/shell/shell heterostructure. This work paves the way for efficient deep-blue-emitting QDs using non-toxic, environmentally friendly compositions.

Supporting Information

Experimental data, PLE spectra, additional absorption, PL, TRPL, and FTIR spectra, XRD data and composition analyses.

Acknowledgements

The authors gratefully acknowledge financial support from Samsung (SAIT GRO grant EQUINOX) and from the French National Research Agency (grant ANR 18-CE09-0039-01 FLUO). We thank Hayley Melville (Moltech, Anjou, France) and CARMA platform from SFR Matrix for the PYSA measurements as well as Stéphanie Pouget for assistance with the X-ray diffraction analysis.

Keywords: colloidal quantum dots • deep blue emission • surface passivation • alumina shell • non-toxic materials

[1] C. Harris, P. V. Kamat, *ACS Nano* **2010**, *4*, 7321-7330.

[2] a) J. M. Pietryga, Y.-S. Park, J. Lim, A. F. Fidler, W. K. Bae, S. Brovelli, V. I. Klimov, *Chem. Rev.* **2016**, *116*, 10513-10622; b) E. Jang, H. Jang, *Chem. Rev.* **2023**, *123*, 4663-4692; c) T. Kim, D. Shin, M. Kim, H. Kim, E. Cho, M. Choi, J. Kim, E. Jang, S. Jeong, *ACS Energy Lett.* **2023**, *8*, 447-456; d) C. R. Kagan, *Chem. Soc. Rev.* **2019**, *48*, 1626-1641.

[3] a) J. Zhou, Y. Yang, C.-y. Zhang, *Chem. Rev.* **2015**, *115*, 11669-11717; b) M. Cardoso Dos Santos, W. R. Algar, I. L. Medintz, N. Hildebrandt, *TrAC, Trends Anal. Chem.* **2020**, *125*, 115819.

[4] C. R. Kagan, L. C. Bassett, C. B. Murray, S. M. Thompson, *Chem. Rev.* **2021**, *121*, 3186-3233.

[5] a) A. Saha, K. V. Chellappan, K. S. Narayan, J. Ghatak, R. Datta, R. Viswanatha, *J. Phys. Chem. Lett.* **2013**, *4*, 3544-3549; b) N. Taghipour, I. Tanriover, M. Dalmases, G. L. Whitworth, C. Graham, A. Saha, O. Özdemir, B. Kundu, V. Pruneri, K. Aydin, G. Konstantatos, **2022**, *32*, 2200832; c) S. Pradhan, F. Di Stasio, Y. Bi, S. Gupta, S. Christodoulou, A. Stavrinadis, G. Konstantatos, *Nature Nanotech* **2019**, *14*, 72-79; d) S. A. McDonald, G. Konstantatos, S. Zhang, P. W. Cyr, E. J. D. Klem, L. Levina, E. H. Sargent, *Nature Materials* **2005**, *4*, 138-142; e) C. Dong, S. Liu, N. Barange, J. Lee, T. Pardue, X. Yi, S. Yin, F. So, *ACS Appl. Mater. Interfaces* **2019**, *11*, 44451-44457.

[6] a) A. Saha, G. Kumar, S. Pradhan, G. Dash, R. Viswanatha, G. Konstantatos, *Adv. Mater.* **2022**, *34*, 2109498; b) G. Xu, S. Zeng, B. Zhang, M. T. Swihart, K.-T. Yong, P. N. Prasad, *Chem. Rev.* **2016**, *116*, 12234-12327; c) A. Saha, G. Konstantatos, *J. Mater. Chem. C* **2021**, *9*, 5682-5688.

[7] a) P. Reiss, M. Carrière, C. Lincheneau, L. Vaure, S. Tamang, *Chem. Rev.* **2016**, *116*, 10731-10819; b) Y.-H. Won, O. Cho, T. Kim, D.-Y. Chung, T. Kim, H. Chung, H. Jang, J. Lee, D. Kim, E. Jang, *Nature* **2019**, *575*, 634-638; c) F. W. Eagle, R. A. Rivera-Maldonado, B. M. Cossairt, *Ann. Rev. Mater. Res.* **2021**, *51*, 541-564; d) S. Tamang, C. Lincheneau, Y. Hermans, S. Jeong, P. Reiss, *Chem. Mater.* **2016**, *28*, 2491-2506; e) R. Yadav, Y. Kwon, C. Rivaux, C. Saint-Pierre, W. L. Ling, P. Reiss, *J. Am. Chem. Soc.* **2023**, *145*, 5970-5981.

[8] a) P. M. Allen, M. G. Bawendi, *J. Am. Chem. Soc.* **2008**, *130*, 9240-9241; b) T. Uematsu, K. Wajima, D. K. Sharma, S. Hirata, T. Yamamoto, T. Kameyama, M. Vacha, T. Torimoto, S. Kuwabata, *NPG Asia Mater* **2018**, *10*, 713-726; c) G. Motomura, T. Uematsu, S. Kuwabata, T. Kameyama, T. Torimoto, T. Tsuzuki, *ACS Appl. Mater. Interfaces* **2023**, *15*, 8336-8344; d) A. C. Berends, M. J. J. Mangnus, C. Xia, F. T. Rabouw, C. de Mello Donega, *J. Phys. Chem. Lett.* **2019**, *10*, 1600-1616; e) D. Moodelly, P. Kowalik, P. Bujak, A. Pron, P. Reiss, *J. Mater. Chem. C* **2019**, *7*, 11665-11709; f) C. Rivaux, T. Akdas, R. Yadav, O. El-Dahshan, D. Moodelly, W. L. Ling, D. Aldakov, P. Reiss, *J. Phys. Chem. C* **2022**, *126*, 20524-20534.

[9] X. Li, X. Gao, X. Zhang, X. Shen, M. Lu, J. Wu, Z. Shi, V. L. Colvin, J. Hu, X. Bai, W. W. Yu, Y. Zhang, *Advanced Science* **2021**, *8*, 2003334.

[10] a) J. Zhang, Y. Yang, H. Deng, U. Farooq, X. Yang, J. Khan, J. Tang, H. Song, *ACS Nano* **2017**, *11*, 9294-9302; b) M. Leng, Z. Chen, Y. Yang, Z. Li, K. Zeng, K. Li, G. Niu, Y. He, Q. Zhou, J. Tang, *Angew. Chem. Int. Ed.* **2016**, *55*, 15012-15016; c) Z. Ma, Z. Shi, D. Yang, F. Zhang, S. Li, L. Wang, D. Wu, Y. Zhang, G. Na, L. Zhang, X. Li, Y. Zhang, C. Shan, *ACS Energy Lett.* **2020**, *5*, 385-394.

[11] a) M. Kneissl, T.-Y. Seong, J. Han, H. Amano, *Nat. Photonics* **2019**, *13*, 233-244; b) Y.-C. Leem, N. Myoung, S.-H. Hong, S. Jeong, O. Seo, S.-J. Park, S.-Y. Yim, J. H. Kim, *Nanoscale Adv.* **2022**, *4*, 3585-3591.

[12] a) C. S. Jung, F. Shojaei, K. Park, J. Y. Oh, H. S. Im, D. M. Jang, J. Park, H. S. Kang, *ACS Nano* **2015**, *9*, 9585-9593; b) C.-S. Yoon, F. D. Medina, L. Martinez, T.-Y. Park, M.-S. Jin, W.-T. Kim, *Appl. Phys. Lett.* **2003**, *83*, 1947-1949.

[13] T. Uematsu, M. Tepakidareekul, T. Hirano, T. Torimoto, S. Kuwabata, *Chem. Mater.* **2023**, *35*, 1094-1106.

[14] C.-H. Ho, H.-H. Chen, *Sci. Rep.* **2014**, *4*, 6143.

[15] A. Aydinli, N. M. Gasanly, K. Gökşen, *J. Appl. Phys.* **2000**, *88*, 7144-7149.

[16] K. Dénoue, F. Cheviré, C. Calers, L. Verger, D. Le Coq, L. Calvez, *J. Solid State Chem.* **2020**, *292*, 121743.

[17] Z. M. Hu, G. T. Fei, L. D. Zhang, *Mater. Lett.* **2019**, *239*, 17-20.

[18] N. Zhou, L. Gan, R. Yang, F. Wang, L. Li, Y. Chen, D. Li, T. Zhai, *ACS Nano* **2019**, *13*, 6297-6307.

[19] F. Dussert, G. Sarret, K. D. Wegner, O. Proux, G. Landrot, P.-H. Jouneau, P. Reiss, M. Carrière, *Nanomaterials* **2022**, *12*, 3703.

[20] a) D. Ren, K. M. Azizur-Rahman, Z. Rong, B.-C. Juang, S. Somasundaram, M. Shahili, A. C. Farrell, B. S. Williams, D. L. Huffaker, *Nano Lett.* **2019**, *19*, 2793-2802; b) M. Zeng, X. Peng, J. Liao, G. Wang, Y. Li, J. Li, Y. Qin, J. Wilson, A. Song, S. Lin, *Physical Chemistry Chemical Physics* **2016**, *18*, 17404-17413; c) S. Zhang, T. Yu, Y. Liu, M. Feng, X. Li, W. Sun, D. Wang, *Chem. Eng. J.* **2022**, *429*, 132248.

[21] W. Huang, L. Gan, H. Yang, N. Zhou, R. Wang, W. Wu, H. Li, Y. Ma, H. Zeng, T. Zhai, *Adv. Func. Mater.* **2017**, *27*, 1702448.

[22] A. N. Yadav, K. Singh, *ACS Omega* **2019**, *4*, 18327-18333.

[23] E. Dhaene, J. Billet, E. Bennett, I. Van Driessche, J. De Roo, *Nano Lett.* **2019**, *19*, 7411-7417.

Entry for the Table of Contents

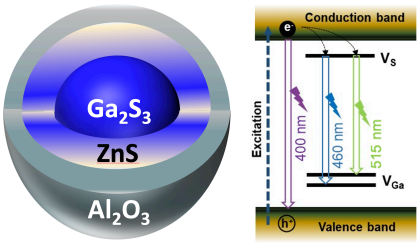

TOC text:

Ga_2S_3 nanocrystals constitute a novel type of quantum dots exempt from toxic heavy metals whose fluorescence can be tuned from broad trap-state to narrow band-edge emission in the deep blue range by coating their surface with a ZnS shell. An additional alumina shell enhances the photoluminescence quantum yield close to 50% while maintaining a short lifetime around 1 ns.

Institute and/or researcher Twitter usernames: peter reiss @peter_reiss